Particle Accelerators, 1996, Vol. 53, pp. 1–34
Reprints available directly from the publisher
Photocopying permitted by license only

FIELD EMISSION STUDIES AT SACLAY AND ORSAY

J. TAN

C.E. Saclay, DSM/DAPNIA/SEA, F-91191 Gif-sur-Yvette Cedex, France

(Received 8 March 1996; in final form 8 March 1996)

During the last five years, DC and RF apparati for field emission studies have been developed at Saclay and Orsay laboratories. Combining these devices, we were able to perform straight comparison between DC and RF field emission from artificial emission sites on the same sample. Other topics are also reviewed: high field cleaning, plausible origins of thermal effects that occurred on emission sites in RF, behaviour of alumina particles under RF field, and optical observations and measurements.

Keywords: Superconducting RF

1 INTRODUCTION

High accelerating fields in superconducting radio frequency (RF) accelerators is mainly limited by enhanced field emission[1] (FE). After their emission by local surface defects and acceleration, electrons impinge the cavity walls and consequently increase exponentially RF dissipation. This limitation for the good running order of the machines motivated an important effort in many laboratories in order to cure cavities of FE. RF field emission studies on accelerating cavities raise many difficulties: diagnostic tools are mainly indirect (by temperature or X-ray mapping[2]), slow turn over, destruction of the cavity for microscopic studies. During the last five years, the GECS (Groupe d'Etudes des Cavités Accélératrices) group at Saclay, and IPN (Institut de Physique Nucléaire) at Orsay have developed DC and RF apparati for FE studies. Coupled together, these devices allow new kinds of experiments on FE in both regimes, without any drawback quoted above.

The present paper will review FE activities in both laboratories since the last workshop. Section 2 presents the whole operating devices, with the last improvements brought. Some previous results (to be continued) are summarized in Section 3 with the appropriate references. In the following sections (4 to 8), we shall review a series of new experimental results on the basic mechanism of RF field emission, as well as on the plausible nature of emission sites with artificially introduced dust contaminant. Then section 9 concludes on these results.

2 APPARATI AND METHODS

2.1 The Global DC Apparatus

A plane parallel gap which can be polarized in DC,[3] is placed in an ultra high vacuum chamber ($< 10^{-10}$ mbar). The maximum electric field available is 50 MV/m when the electrode separation is 0.5 mm. The very low FE regime ($10^{-18} - 10^{-12}$ A) is investigated by means of an electron multiplier placed behind a grid anode. This latter is replaced by a massive stainless steel anode on a picoammeter for higher detected currents. The recent addition of an external lamp allows samples' heating up to 300°C by radiation through a window (Figure 1).

2.2 The Modified SEM

This apparatus consists of a scanning electron microscope (SEM) modified for FE studies.[4] It is equipped with a polarized tungsten anode (tip radius 20 μm) scanning above a broad area cathode surface at a distance of $\sim$ 50 μm. The applied field ranges from 0 to 200 MV/m with a working pressure of $\sim 10^{-6}$ mb. This device allows a complete characterisation at the microscopic level of individual emitter site present on the cathode surface: study of its morphology, current FE measurements monitored with a picoammeter and chemical composition analysed with an EDX facility (Figure 2).

2.3 The 1.5 GHz Re-entrant Cavity

The "warm" cavity[5] made of copper-plated stainless steel is inspired from U. Klein's cavity.[6] It is designed so as to have a strong electric field

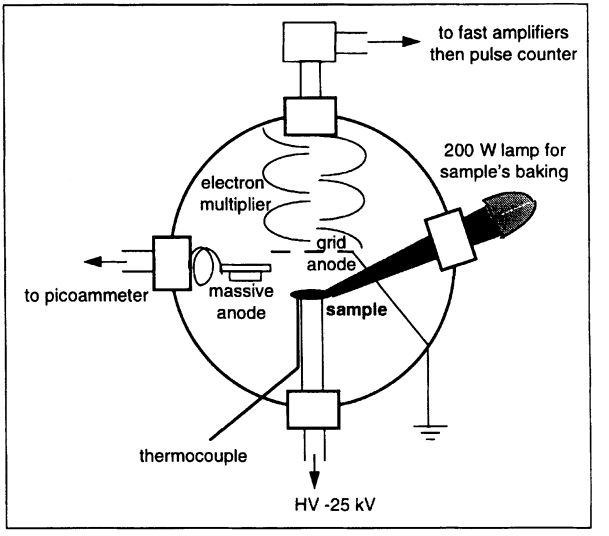

FIGURE 1 Ultra high vacuum chamber housing the global DC apparatus.

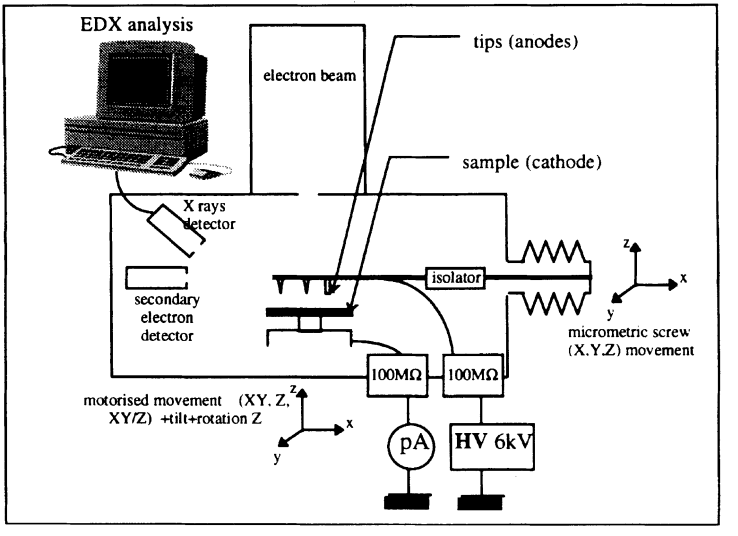

FIGURE 2 Scanning electron microscope modified for field emission studies.

enhancement at the top of a removable sample (Nb, Cu, ...). Electrons originating from the sample surface are collected by an antenna placed 12 mm afar from it, thus measuring an integrated intensity with a picoammeter. RF power is supplied by a 5 kW klystron working in a pulse mode with pulse lengths in the range 10 μs – 10 ms. In order to avoid strong power dissipation on the cavity walls, the duty cycle must be kept lower or equal to 1%. The choice to work at room temperature, however, allows a fast turnover of the experiments. The maximum surface peak field achievable is related to the geometry and the sample material. With a Cu sample of type #1, the maximum surface field that can be applied is 60 MV/m on 10 mm^2, whereas it reaches 110 MV/m with a type #2 sample. However, high surface fields is paid by the reduction of the studied area down to 2 mm^2 (see below).

When not explicitly mentioned, sample of type #1 is used. The experimental set up is schematically represented here.

An optical measurement facility has been developed[7] by I.P.N. at Orsay for quantitative study of light emission. For that purpose, the warm cavity has been slightly modified by addition of a sapphire window facing the sample surface (Figure 5). An intensified camera records the light emitted by the sample. The camera has a sensitivity of 5×10^{-4} lux in the wavelength range 400–650 nm. Individual light spots are selected by placing a square diaphragm (50×50 μm). The spectral analysis system consists of a cooled CCD multichannel sensor integrating the incoming light dispersed by a prism located on the optical path. The CCD detector covers the wavelength range 400–1100 nm. The whole acquisition data has been computerised and camera images are recorded during the experiment. This device, recently improved, allows real time analysis of optical radiation associated with FE measurements.

3 SUMMARY OF THE PREVIOUS RESULTS

Before giving a full account of the new experimental results obtained with the whole apparati described above, we shall summarize here some previous ones with the appropriate references.

Niobium sheets ($\sim$ 1 cm^2) with various surface treatments as chemical etching, electropolishing, or oxide coating by anodization, have been tested in the global DC apparatus.[3] It appeared that the first I(E) curve with increasing

Sample	*# 1*	*# 2*
Copper	60 MV/m	110 MV/m
Niobium	45 MV/m	95 MV/m

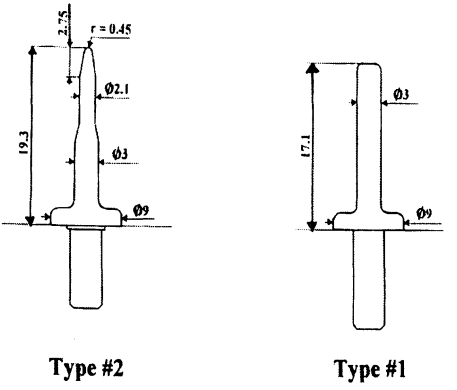

FIGURE 3 Sample geometry (all dimensions in mm) and maximum peak field for 5 kW input power.

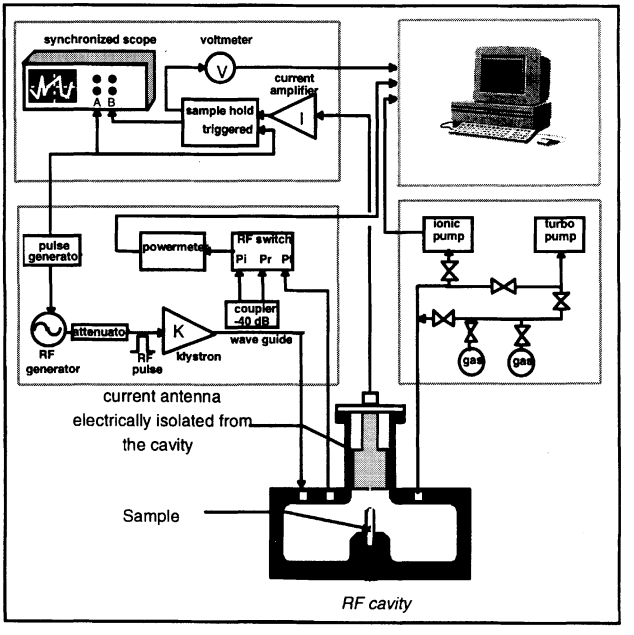

FIGURE 4 Experimental set up of the 1.5 GHz re-entrant cavity.

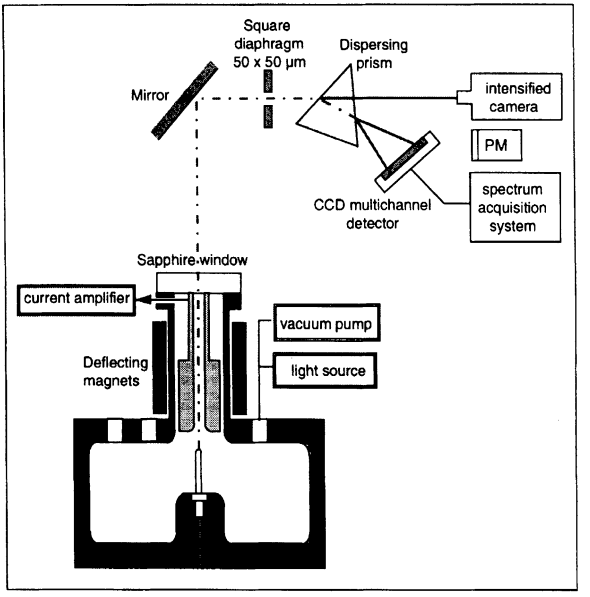

FIGURE 5 Optical system for light spots observation and spectral analysis in the "warm" cavity.

field was always accompanied by high current instabilities, caused by some kind of surface processing. Fowler-Nordheim (FN) plots obtained seemed to be composed with a superposition of two regimes: the low current part providing high field enhancement factor ($\beta \sim 500$–600) with unrealistic emitted area S smaller than the atomic size, and the high current part giving "standard" values. Further, it was observed that the FN slopes extracted from anodized samples were not affected by the oxide thickness in the range 5–342 nm.

It has been clearly shown that emitter sites on clean surfaces are related with some kind of surface defects, such as contaminants of foreign species or scratches.[8–10] For difficulties raised in the study of natural emitters (no clear cut zoology, current instabilities and irreversible damages before their characterisation, e.g. in RF cavities), we focussed the following studies on well known, well controlled artificial emitters. Those sites are produced either by sprinkling particles on the surface, or by scratching the surface with a diamond needle.

On one hand, scratches performed on samples previously free of detectable FE,[11] as well as irregularly shaped metal particles (Fe, Ni, Au, Ag) lying on Nb substrates are strong emitters both in DC field[12] **and in RF** (with Fe particles).[13] Furthermore, after occurrence of a spark with a previously identified emitter site, then apex of a scratch is seen to be melted. On the other hand, it is found that particles with insulating oxides (Nb, Ti), spherical particles (Fe, Ni), and insulating particles (Al_2O_3, SiO_2) reveal no emission up to DC fields as high as 100 MV/m. Those results lead the authors to revisit the projection model. The FE originating from these surface defects may be explained by assuming superposed geometrical protrusions.[11]

The behaviour of iron particles is somewhat different when submitted to RF field. Indeed, after an RF test, the main features deduced from SEM observations are:

(i) some particles disappear, generally leaving in their place small craters ($\sim 5\ \mu$m) on the surface,
(ii) the remaining particles are lined up along the electric field, perpendicular to the surface, thus maximizing the electric field enhancement factor,
(iii) their bases are generally molten leaving them well stuck with the metal surface.[8]

A Cu sample scratched with a *W* needle has been mounted in the "optical" cavity.[14] Light spots detected by the photomultiplier (PM) occurred at a field level of 20 MV/m, whereas the sensivity of the CCD camera allowed optical detection at 35 MV/m. The time response of the spots was completely correlated in shape and length with the RF pulsed power. Intensity of the radiation vs $1/\sqrt{E_{\text{peak}}}$ representation provided linear fits, which might be interpreted as electroluminescence or black body radiation phenomenon. The first light spectra obtained using a series of wide bandpass filters provided a peaked structure in the range 600–750 nm. However no clear correlation was found between light emitters and electron emitters.

4 FIELD EMISSION IN DC AND RF REGIMES

4.1 Introduction

DC FE from large area electrodes has been widely studied, whereas most RF studies on this theme have been indirect.[2] However, RF FE characteristics are close to those obtained on broad area electrodes under DC field, i.e.

local phenomenon and linear shape of the FN plots. If one excepts the result of Klein *et al.*[6] who showed the absence of correlation between β and the frequency of the RF field (range 0.5–3.5 GHz), the relation between DC and RF FE is not always clear. Here we present the results of the first detailed comparison between DC and RF, and in particular on the same sample studied in both domains. As removable samples of the cavity can be tested in the modified SEM, these complementary tools have been associated. For that purpose, we use Nb samples, initially emission-free, with a unique geometrical defect produced artificially.

First of all, a crucial point about data analysis is to be emphasised. Indeed, the comparison of I(E) curves obtained in DC and RF cannot be done directly as it is shown that the pre-exponential factor of the FN equation differs between the two regimes. Assuming that FE is instantaneous and occurs in a quasi static electric field, the relationship of FE in DC[1] and RF[5] regimes are respectively given by :

$$I_{DC} = \frac{A}{\phi} S_{DC} \cdot (\beta_{DC} E_{DC})^2 e^{-\frac{B\phi^{3/2}}{\beta_{DC} E_{DC}}}$$

$$I_{RF} = \frac{C}{\phi} S_{RF} \cdot (\beta_{RF} E_{RF})^{2.5} e^{-\frac{B\phi^{3/2}}{\beta_{RF} E_{RF}}}$$

$$\text{with } C = \frac{2\sqrt{2}}{3\pi} \cdot \sqrt{\frac{\beta_{RF}}{B\phi^{3/2}}}$$

where I is the emitted current in ampere, E the macroscopic surface field in V/m, S the emitting area in m^2, ϕ the work function in eV and β the field enhancement factor. A and B are numerical constants equal to: $A = 1.54 \times 10^{-6}$, $B = 6.83 \times 10^9$. In fact (β, S) *parameters are the only ones comparable in our experiment.* FE measurements are far more reproducible in the cavity than in the modified SEM. So if we place the deduced (β_{RF}, S_{RF}) parameters in the I_{DC} equation giving $I_{DC} = f(E_{DC}, (\beta_{RF}, S_{RF}))$, it is possible then to superpose this curve with the DC measurements. These curves should be the same if one assumes the identical basic FE mechanism in DC and RF regimes.

4.2 Results

After scratching the sample inside the SEM, FE measurements are performed without breaking the vacuum in the SEM chamber, and they become unstable

when the current level exceeds 1 nA. The results obtained with the cavity are as follows: $\beta_{RF} = 158$ and $S_{RF} = 1.04 \times 10^{-15}$ m^2. The maximum intensity collected with the antenna is 1.47 μA at 46.3 MV/m peak field. Then the sample is replaced once in the SEM for observation and new DC tests. The morphology of the defect is unchanged. The typical results are presented in Figure 6 and in Figure 7.

4.3 Discussion

When examining the low current part (< 1 nA) of 5 DC curves out of 8, it appears that the FE characteristics of the emitter site are very close to the theoretical FN one with (β_{RF}, S_{RF}), as reported in Table I. Other samples tested that way give similar results. Thus, the FE mechanism seems to be the same in DC and RF domains. Moreover, simple theoretical considerations with the Heisenberg incertitude relation or with the Keldysh theory[15] show that the hypothesis of a quasi-static phenomenon is fully justified at microwave frequencies.

The remaining discrepancies may be explained by the presence of adsorbed gases on the sample surface (no baking system) whereas RF dissipation on the cavity walls contribute to desorb the surfaces. The role of adsorded gases on FE is clearly demonstrated in Figure 8 representing the FE current vs time recorded at constant field level, under ultra high vacuum conditions. After a baking cycle, the gain on current stability was so that the standard deviation decreases down to 1%.[16] Thanks to this improvement, new experiments on comparison of RF and DC field emission will soon be undertaken in order to obtain more definite conclusions.

TABLE I Characteristics of an emitter site on a Nb sample tested alternatively in DC and RF devices. The work function is taken equal to 4 eV

	DC data at low current level before RF test	*RF data*	*DC data at low current level after RF test*
β	164	158	154
$S(\times 10^{-15}$ m$^2)$	0.4	1	1.4

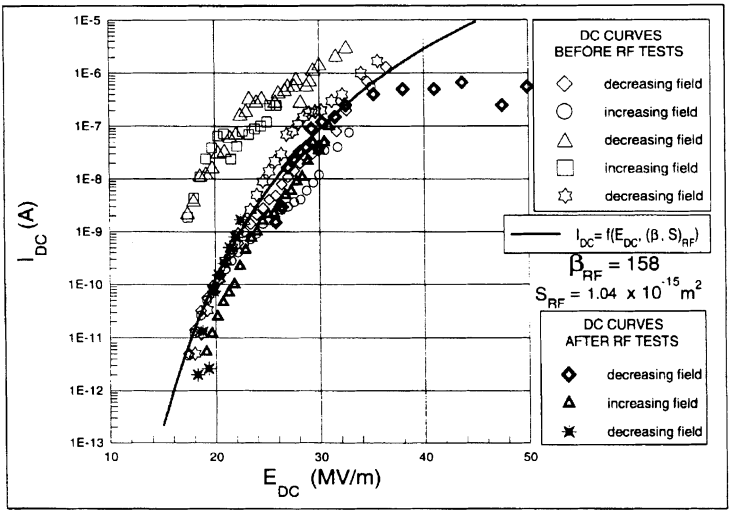

FIGURE 6 Comparison of $I_{DC} = f(E_{DC}, (\beta_{RF}, S_{RF}))$ curve with ones obtained with the modified SEM.

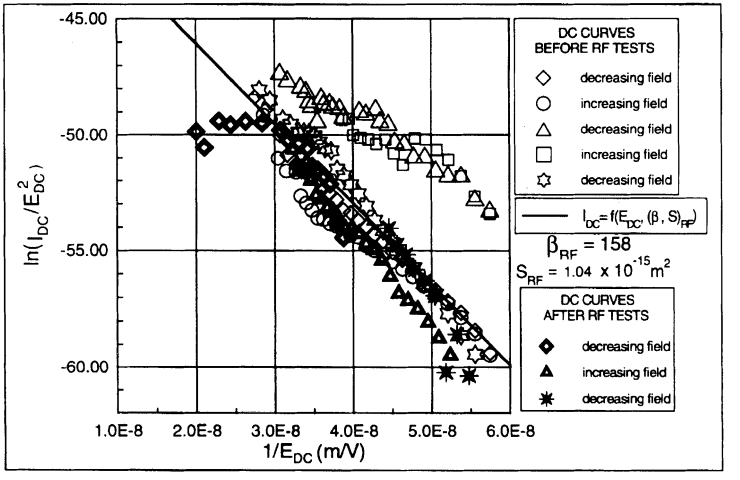

FIGURE 7 Comparison of $I_{DC} = f(E_{DC}, (\beta_{RF}, S_{RF}))$ curve with ones obtained with the modified SEM: corresponding Fowler-Nordheim plots.

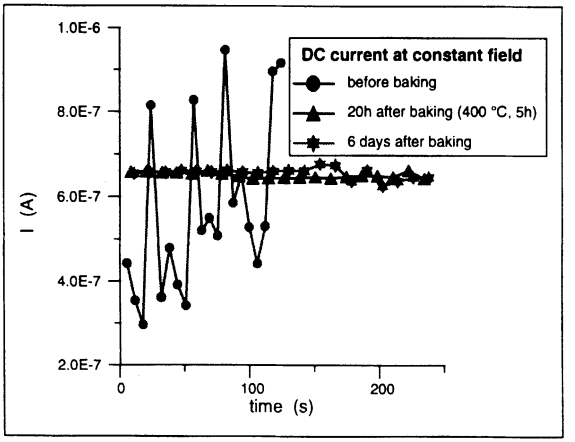

FIGURE 8 FE current vs time at constant field level, under ultra high vacuum conditions: role of adsorbed gases before and after a baking cycle.

5 HIGH ELECTRIC FIELD CLEANING

5.1 Aim of the Experiment

FE on RF surfaces is mainly concerned with dust particles. At Cornell, Auger measurements revealed foreign species in each of 29 craters.[17] Most of elements detected, such as Fe, Cr or Si may be related to the cavity environment (chemical bath, cleanroom atmosphere, mounting steps...). Cleaning the surfaces of RF cavities is thus necessary. Many surface treatments, like firing, high pressure water rinsing or high pulsed power RF processing, have already been applied.[18] For this latter, it is generally believed that RF processing reduces FE by inactivation of emitting sites via a mechanism of thermal instability, followed by a microdischarge destroying the site. This mechanism is certainly at work to reduce FE but we would like to show that pulse processing is also effective to remove mechanically dust particles, thereby reducing the total FE from the surface.

In previous experiments, Nb samples were intentionally contaminated with iron particles, and tested in the cavity. We noticed incidentally at that time that the number of remaining particles on the surface after applying the RF power was related to the pulse length.[13] Following these observations, we

wished to undertake a more systematic study in order to lighten the basic mechanism of cleaning dust particles by RF pulses. Three parameters appear to be of major importance: the field level on the surface, the RF pulse length τ, and the duration of the experiment or the total number of pulses.

5.2 Samples' Preparation and Procedures

As we wish to observe a statistical behaviour of dust particles, hundreds of irregular Fe particles (20 μm mean size) are sprinkled on chemically etched niobium samples. In our experiment, RF duty cycle is always kept equal to 1%. The reference number of particles is arbitrarily taken to be 100% after an initial low RF field test (< 5 MV/m), so as to get rid of uncertainties due to poorly adhering particles that can get lost during the transportation between the SEM and the cavity.

5.3 Field Level and RF Pulse Length Effects

The study of the field level effect should inquire about the minimum value of the surface field for particles removal and for an irreversible damage either by welding the particles or by leaving craters on the surface.

Four niobium samples prepared so have been tested in the cavity with a constant duty cycle of 1%, but the pulse length was different for each sample. It is in the range of 10 μs to 10 ms. All samples were RF processed at a low field level for 30 mn then removed for SEM observation and for particles numbering before applying the higher RF field. Thus all samples experienced successively 5, 14, 30 and 45 MV/m for 30 mn each time. The results are summarized in Figure 9.

As one could expect, the stronger the field, the lower the number of remaining particles and consequently the more efficient the cleaning is. More interesting is the fact that at a given field, the shorter the pulse length the better the processing is.

SEM observations of the samples surface are interesting. A few particles start to stand up along field lines at 5 MV/m. At 30 MV/m, first craters appear on samples processed with the largest pulse lengths (τ = 1 ms and τ = 10 ms). Their locations are always related to missing iron particles, confirmed by EDX analysis. At 45 MV/m, the number of craters increases with τ.

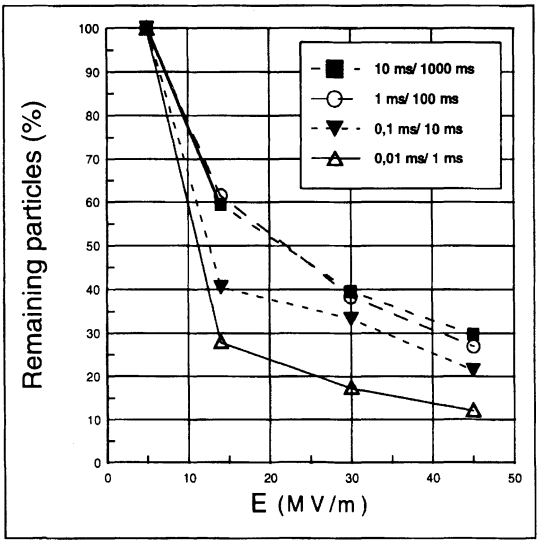

FIGURE 9 Dust-cleaning efficiency as a function of the applied electric field.

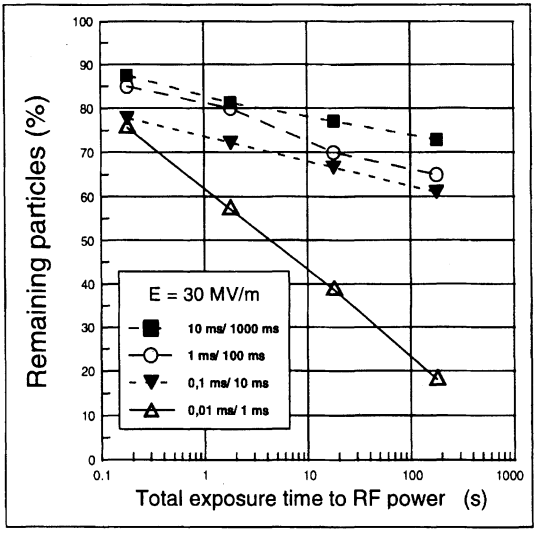

FIGURE 10 Dust-cleaning efficiency as a function of processing time.

5.4 Time Processing and RF Pulse Length Effects

Four other samples are prepared following the same procedure described in Section 5.2. We wish to observe whether the total number of applied RF pulses (or processing duration) can modify the number of remaining particles. To do so, all RF tests are done at a constant field level equal to 30 MV/m. Then different time durations are applied on the same sample. After each test, the sample is dismounted for particles' numbering in the SEM. The results are summarized in Figure 10.

They first confirm the importance of the pulse length that has been already pointed out in the previous graph. Short RF pulses are far more efficient than long ones. Moreover, one sees that there is a very strong *cumulative effect* at any pulse length: the cleaning of the surfaces continues as long as the RF power is applied.

Micrographs of the top of two niobium samples after processing for 5 hours are shown below. The efficiency of processing with short RF pulses ($\tau = 10$ μs, Figure 11b) as compared with long RF pulses ($\tau = 10000$ μs, Figure 11d) is illustrated here, although the field level was the same for both samples. It should also be noted that the surface is much more damaged ($\sim$ 100 craters and some molten particles) when processing with long pulses, than with short ones (5 craters).

5.5 Discussion

The first series of tests confirms the need for high electric fields to overcome adherence forces. Electric force can be evaluated by considering electric pressure acting on a conducting particle. It is of order: $F = \pi \cdot \varepsilon_0 \cdot h^2 E^2$, and depends quadratically with the height h of the particle and with the surface macroscopic electric field E. Comparison between this (repulsive) electric force and the adherence force acting on the particle[19] shows that micron-sized particles can plausibly be removed by the RF field, thereby giving credit to our explanation of the RF cleaning (see Figure 12).

The second series of experiments suggests that particles removal occurs via a cumulative effect, and demonstrate that the mechanical action of short RF pulses is not equivalent to a long one. It can be understood by the characteristic time for thermal equilibrium which was numerically evaluated to 1 ms.[14] A further experimental confirmation is given in the following section. So short RF pulses prevent thermal effects that may lead to melting and consequently

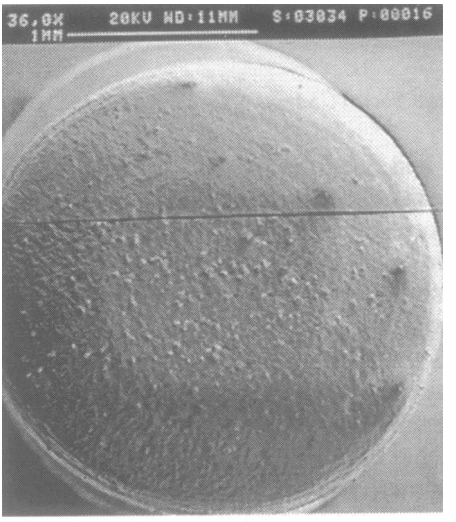
36,0X 20KV WD·11MM S·03034 P·00016
1MM

(a)

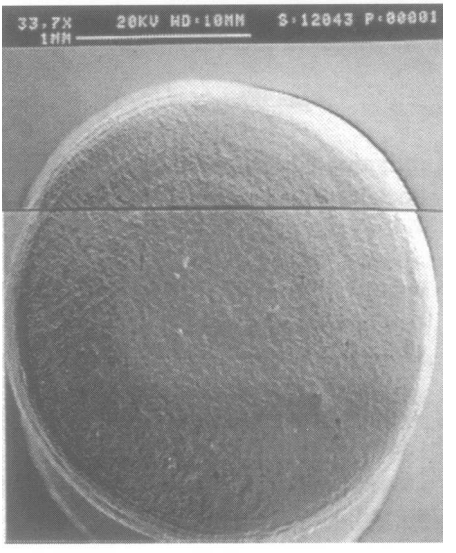
33,7X 20KV WD·10MM S·12043 P·00001
1MM

(b)

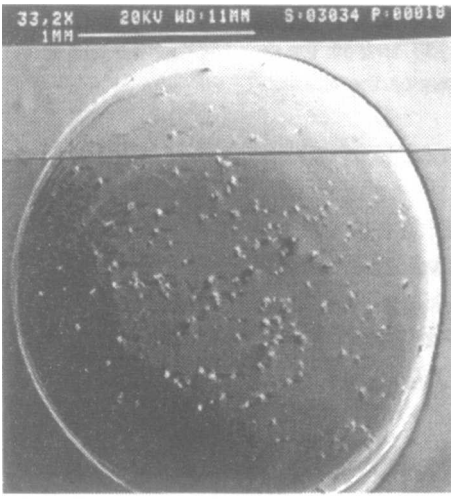

(c)

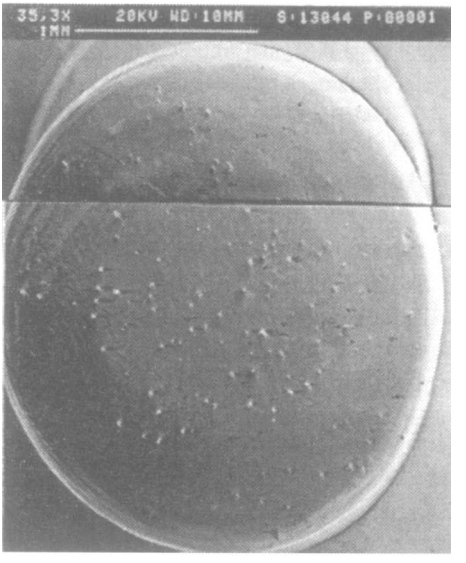

(d)

FIGURE 11 Efficiency of short RF pulses and long time processing (5 hours). Before processing in 11(a), and after processing with $\tau = 10$ μs in 11(b). Before processing in 11(c), and after processing with $\tau = 10000$ μs in 11(d).

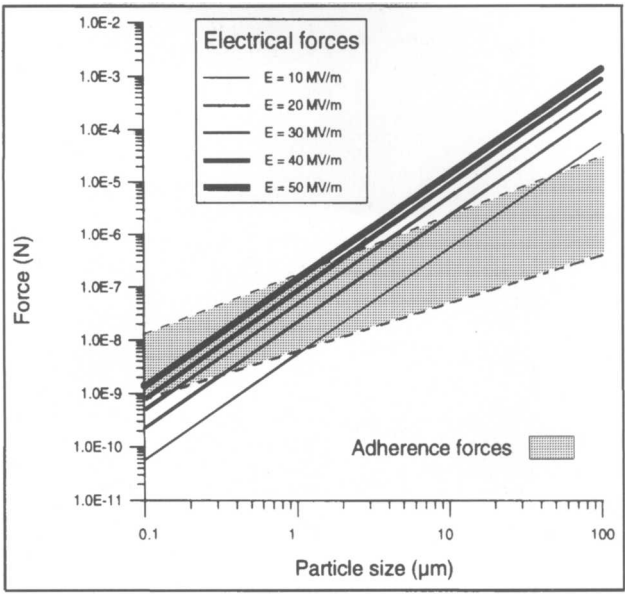

FIGURE 12 Electric force and adherence forces represented as a function of the particle size.

welding particles onto the surface. As shown in this work, dust contaminated surfaces may be cleaned by RF pulses. Three conditions are required for a more efficient processing:

- a large number of pulses to obtain cumulative effect,
- processing with short pulses to avoid thermal effects,
- applying a high enough peak field to overcome adherence forces.

6 CONTACT THERMAL RESISTANCE MEASUREMENTS

6.1 Thermal Effects in the Cavity

Important thermal effects arise on particles during RF processing[8] (see Figure 13). The poor thermal contact between the particle and the substrate probably influences the thermal behaviour of the system. A quantitative analysis of this behaviour requires the knowledge of this important parameter.

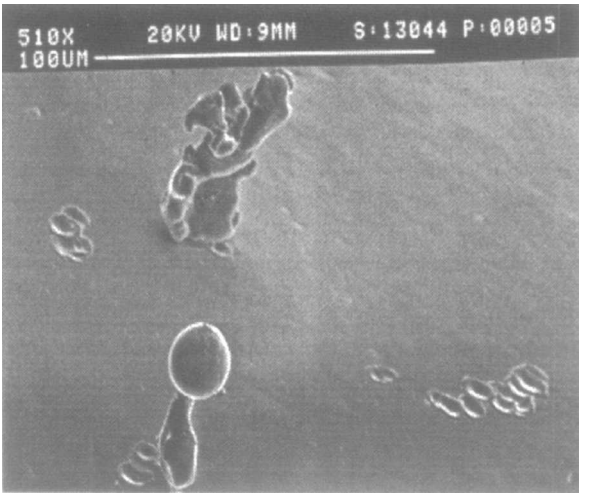

FIGURE 13 Thermal effects that may occur to Fe particles: $E_{RF} = 30$ MV/m, duty cycle = 10 ms/1000 ms.

A new experimental method allowing measurements of the contact thermal resistance between particle and substrate is presented in the following.

6.2 Experimental Procedure

The principle of the experiment consists of heating gradually a particle with a controlled power supply and noting the minimum power P necessary to melt it. Thus one may deduce the contact thermal resistance R_c with the following relationship

$$R_c = \frac{T_{\substack{\text{melting point} \\ \text{of the particle}}} - T_{\text{substrate}}}{P}$$

(see also ref 20).

For that purpose, we use the primary electron beam of the SEM to fire a metallic particle lying on the substrate. The SEM (Cambridge Stereoscan 120) provides a maximum current beam of 3 μA by modifying standard working conditions, i.e.

(1) applying a maximum filament-anode voltage (30 kV here),
(2) placing the largest final diaphragm (140 μm) and

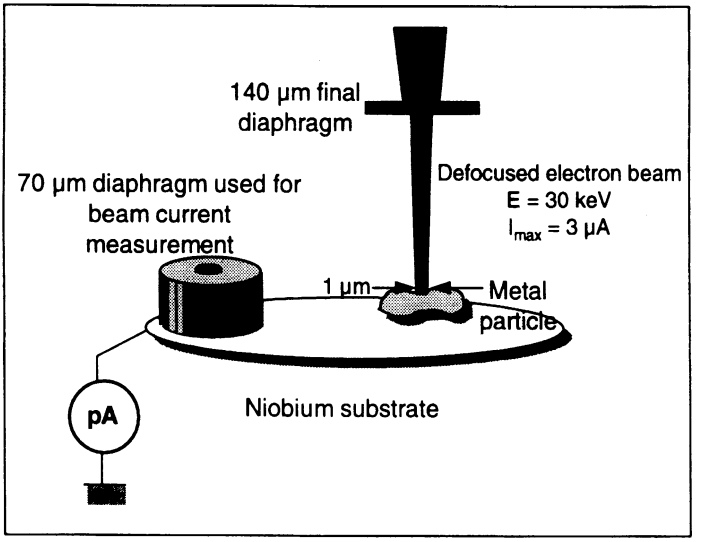

FIGURE 14 Operating conditions for firing particles with the SEM electron beam.

(3) reducing the resolution far below the cut-off point. However the price for high intensity is a very poor resolution as the beam cross-section increases[21] from ~ 5 nm to ~ 1 μm.

For electron bombardment, a beam spot mode is to be used. This mode is approached by focusing on the particle at the highest magnification, so that in practice a micron sized beam scans over a restricted area of ~ 0.25 μm^2 of the particle for 30 s. By the same way, the stable beam current is first recorded with a Faraday cup (70 μm metal diaphragm) and a picoampere meter (Figure 14).

Iron particles as well as Niobium particles are sprayed on a Nb substrate. The penetration depth in matter for 30 keV electrons for both metals[22] is respectively 3.46 μm and 3.76 μm. So one may assume that the whole energy is deposited in 20 μm sized particles. Losses due to primary back scattered electrons and radiation are taken into account for the effective incident power calculations. Some physical characteristics are summarized in Table II.

TABLE II Physical parameters needed to deduce the effective incident power deposited by 30 keV electrons on 20 μm sized metal particles (Fe and Nb)

	Fe	*Nb*
Melting point	1808 K	2741 K
Proportion of back scattered electrons at 30 keV	0.25	0.35
Maximum radiation losses at melting point	0.11 mW	0.6 mW
Electron penetration depth at 30 keV	3.46 μm	3.76 μm

6.2.1 Results

For 20 μm sized iron (resp. Nb) particles, there is no apparent change below the threshold power of 10 mW (resp. 15 mW). The power necessary to melt them is in the range 10–15 mW (resp. 15–20 mW). Twenty particles of each material have been melted with the electron beam. Although this method is destructive for particles, it is possible for the first time to determine the contact thermal resistance at a microscopic level.

$$\textbf{Fe particles } 10^5 \text{ K.W}^{-1} < R_c < 1.4 \times 10^5 \text{ K.W}^{-1}$$

$$\textbf{Nb particles } 1.3 \times 10^5 \text{ K.W}^{-1} < R_c < 1.6 \times 10^5 \text{ K.W}^{-1}$$

Micrographs of particles before and after firing are shown in Figure 15 and Figure 16. It is also important to note that after being melted, a further increase of power up to 100 mW does not change the shape of the particle anymore. This fact is easily interpreted as a large increase of the thermal contact at the particle-substrate interface when the particle starts to melt.

6.2.2 Discussion

The characteristic time for thermal equilibrium of the particle is related to its volume, its specific heat and R_c, and is expressed as: $\tau = R_c.C.V$. Taking $V \sim 10^{-14}$ m^3, $C = 10^6$ J/K/m^3, and the measured R_c, one finds a value of

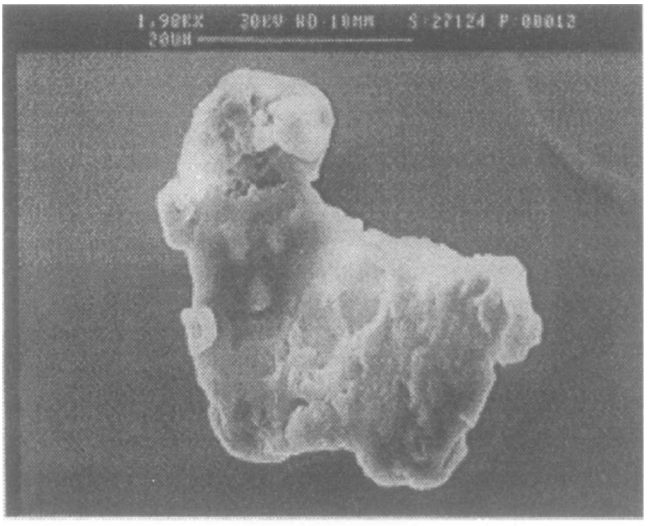

(a)

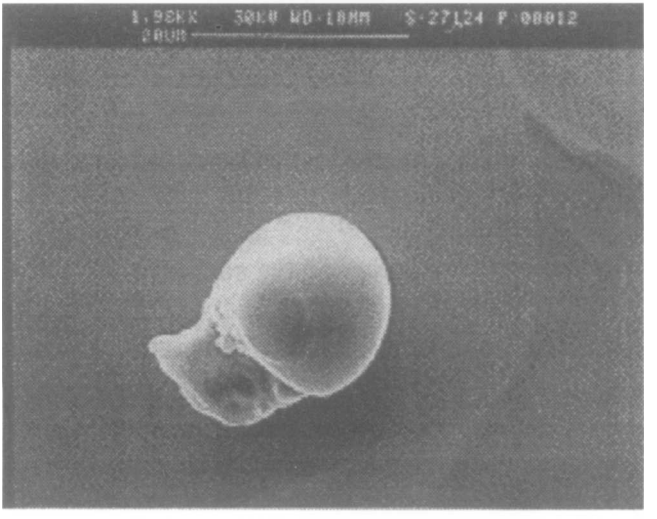

(b)

FIGURE 15 Fe particle micrographs (a) before, (b) after exposure to a 14.9 mW electron beam.

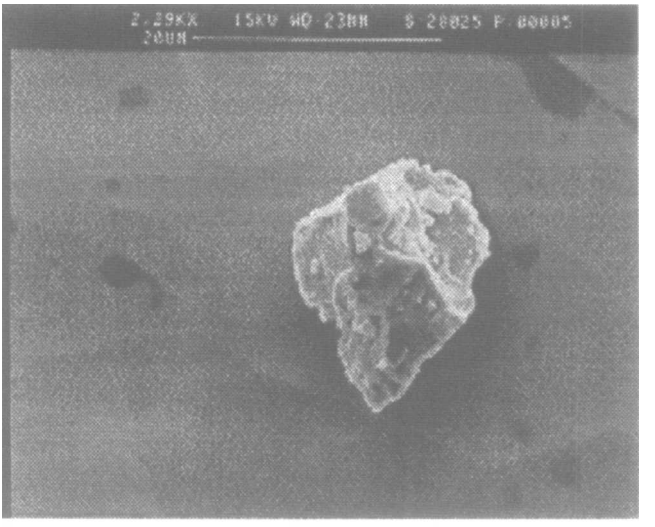

(a)

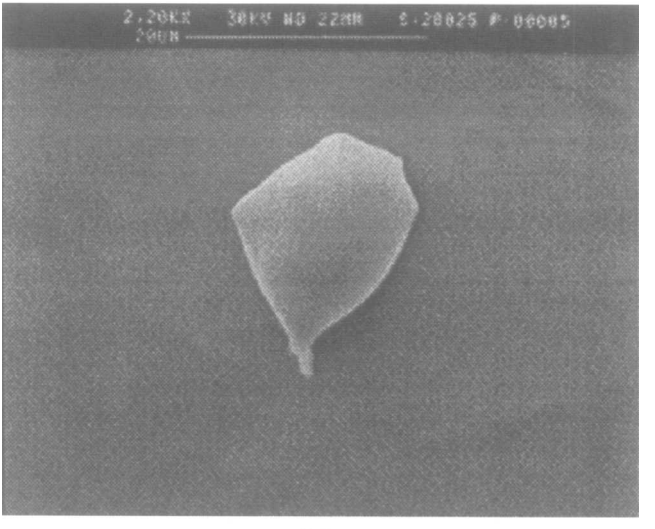

(b)

FIGURE 16 Nb particle micrographs (a) before, (b) after exposure to a 18.9 mW electron beam.

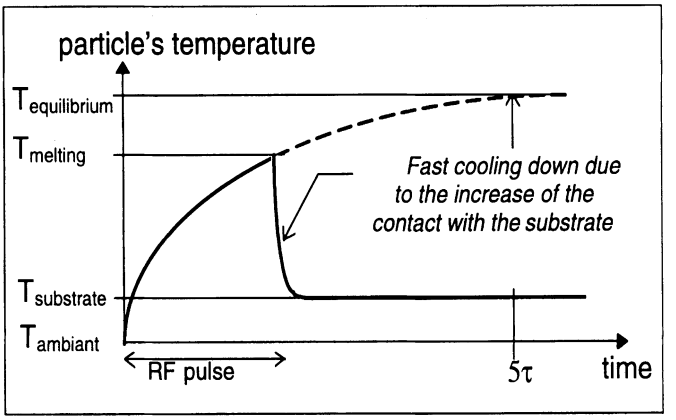

FIGURE 17 Particle's temperature as a function of time.

τ close to one millisecond. Now it is shown in the previous section that RF pulse length at which the polluted samples undergo a violent thermal process was 1 ms at a surface field level of $\sim$ 30 MV/m.

This means two things:

(1) the melting point is reached during the RF pulse,
(2) the equilibrium temperature is certainly higher than the particle's melting point.

So the probable evolution of the particle's temperature during a RF pulse is represented in Figure 17. The results discussed here are consistent with those obtained on the previous study of pulse processing. Schematically by shortening RF pulse length far below the characteristic time for thermal equilibrium, melting of particles is avoided, whereas processing with RF pulses much longer than the characteristic time leads to strong thermal effects.

The minimum power level needed to melt a metal particle can thus be determined, and is of order: $P = \dfrac{T_{\text{melting point}}}{R_c} \approx \dfrac{2000}{10^5} = 20$ mW. This power cannot be provided by RF heating or Joule effect due to field emission itself. Nottingham effect is equally unable to deliver this amount of power.[23] In our view, the only plausible cause of heating is ion bombardment induced by desorption or evaporation from the emitter. However as the local pressure is unknown, further experimental investigations should be undertaken to confirm this hypothesis.

7 ALUMINA PARTICLES

7.1 Alumina Particles Under RF Field

When electrically stressed in the modified SEM, insulating particles (Al_2O_3, SiO_2) lying on Nb substrate revealed no FE up to 100 MV/m, as opposed to metal particles.[12] It was concluded finally that *dust* emitting sites consist mainly of irregularly shaped conducting particles. After a confirmation under RF field with iron particles, we wish to check the harmlessness of insulating particles under high RF field. So, a niobium sample *previously free of detectable FE* in the cavity, has been contaminated with 50 μm sized alumina particles (the same origin like those used by Jimenez *et al.*). After examination in the SEM, the sample was mounted in the cavity for a test (duty cycle = 3 ms/800 ms).

7.1.1 Observations During RF Test

While increasing slowly the RF power in the cavity, some processing events take place at 7 MV/m. Moreover, a FE current of 600 pA is recorded at 8 MV/m. At higher field levels, we can note strong current instabilities. But after processing, the sample emits a stable current of 160 nA at 47.5 MV/m. *Reversible and reproducible* current vs field characteristics are obtained, even after removal for SEM observations and after exposure to air for a couple of days. However, a modification in the duty cycle (30 ms/4 s) produces an irreversible change of the characteristics (see curves #a and #b of Figure 18). Curve #c represents measurements made with another sample prepared the same way.

The major information brought by this experiment is that alumina particles emit like metallic ones under RF field with an *exponential law for the current versus field curves*. At least, it is shown here that insulating particles can be classified as RF field emitter sites.

7.1.2 SEM Observations after RF Test

Details of modifications that happened to alumina particles after RF test are shown in the next figure. Most of conglomerated particles had exploded into thousands of minute ones ($\sim$ 0.2 μm sized). Some of those seemed to be lined up along electric field (without any piling effect) but their shape

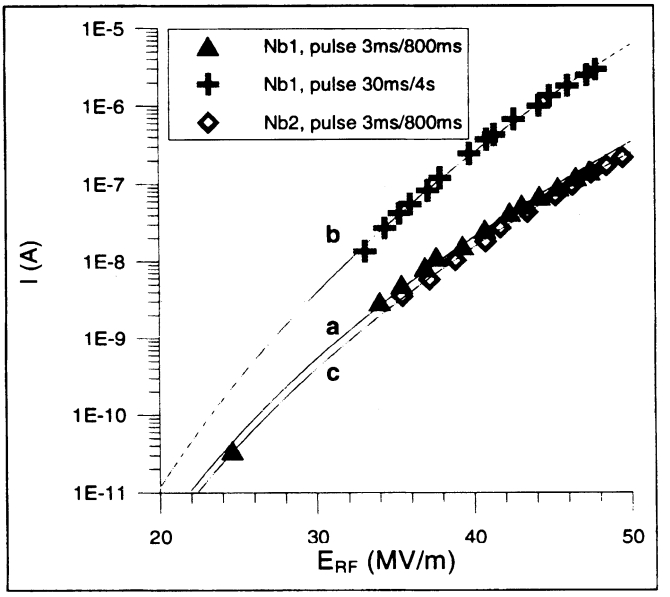

FIGURE 18 RF FE from Al_2O_3 particles sprayed on Nb samples. #Nb1: curves a and b; #Nb2: curve c.

has been completely modified. The occurrence of thermal effects as melting and welding of particles on the sample surface, is illustrated in the last micrograph. It is interesting also to note the lack of ≪ black halo ≫ under particles submitted to the SEM beam, whose presence characterize charge effect of dielectric materials. Five small craters ($\sim$ 5 μm sized) were found on the sample surface.

7.1.3 Location of Emitters Sites in the SEM after RF Test

The polarized anode tip scanning above the sample surface has located three emitter sites. Electrons seemed to originate from heaps of tiny alumina particles, and not from previously identified craters. The threshold fields for an emission of 10 pA are in the range of 24–42 MV/m. However it was not possible to determine whether alumina particles or something else hidden below those was field emitting.

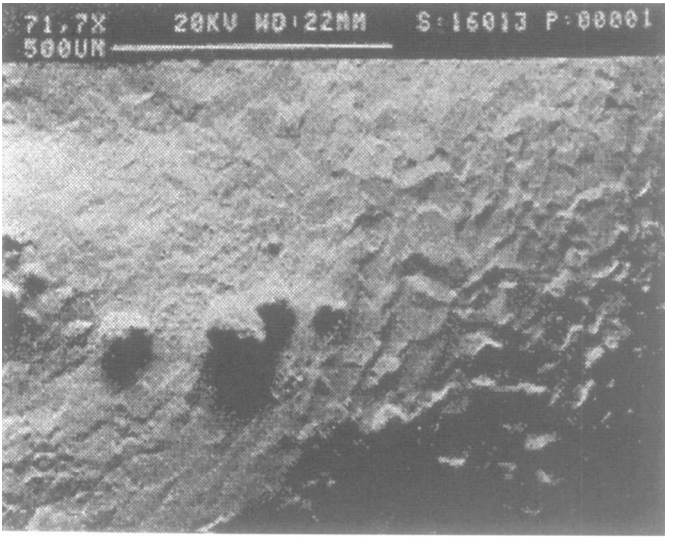
71.7X 20KV WD:22MM S:16013 P:00001
500UM

(a)

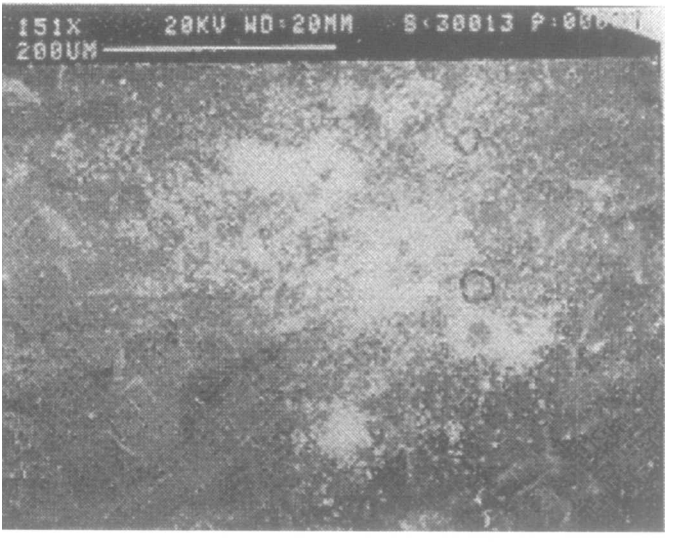
151X 20KV WD:20MM S:30013
200UM

(b)

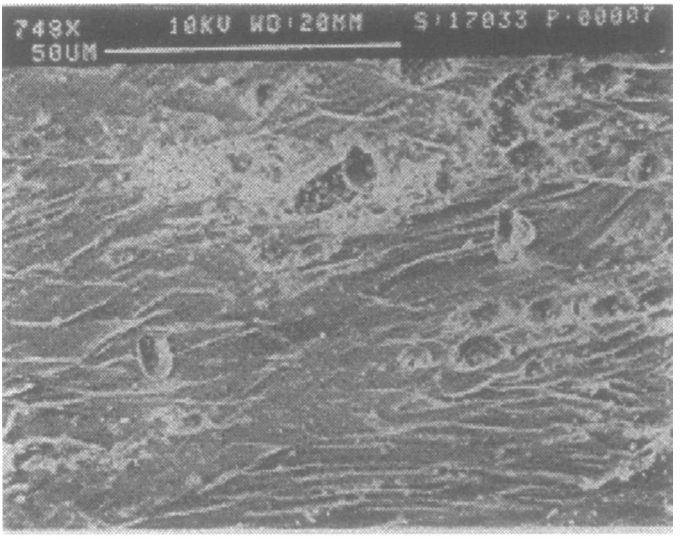

(c)

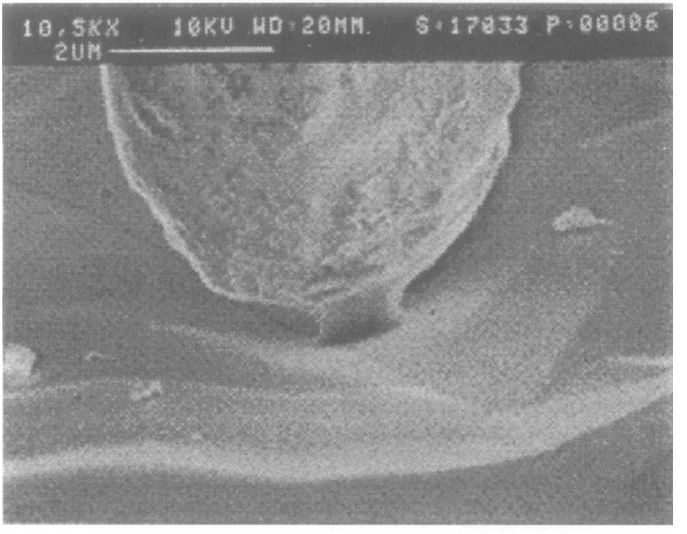

(d)

FIGURE 19 Alumina particles before (a) and after RF test: (b) particles exploded, (c) lined up, (d) melted and welded.

FIGURE 20 Alumina particle melted after 0.25 mW electron bombardment.

7.2 Contact Thermal Resistance Measurements of Alumina Particles

The new method for measuring the contact thermal resistance was also applied to these particles. Surprisingly, it was found that only 0.25 mW of effective incident beam power was necessary to melt 20 μm sized particles (melting point: 2345 K). This provides an R_c value two orders of magnitude higher than for metal particles, i.e.:

$$\mathbf{Al_2O_3 \text{ particles } R_c \sim 10^7 \text{ K.W}^{-1}}$$

A micrograph of molten alumina particle is shown in Figure 20.

7.3 Discussion

Some hypothesis may be proposed to explain our observations.

FE from our samples contaminated so can originate from an external contaminant, present either in our powder or fell down onto the surface during transportation steps. However EDX analysis revealed nothing but Nb, Al and O (with the resolution of this facility) on both samples tested. Further, craters found were not close to emission sites.

The RF power dissipation relationship for dielectric materials is proportional to the cube of the particle size ϕ: $\overline{P}_{RF} \approx \frac{1}{2}\omega \cdot \text{tg}\,\delta \cdot \varepsilon_0 \cdot \varepsilon_r \cdot E_p^2 \cdot \phi^3$, where ω is the angular frequency equal to 10^{10} in our case , tg δ the loss tangent. If we assume values of 10^{-3} for tg δ, 9 for ε_r and a RF field level E_p of 20 MV/m one finds that the power deposited in the 20 μm sized particle reaches 0.2 mW. Note that the electron beam power to melt them was 0.25 mW. One may deduce that under RF field, alumina particles are close to their melting point, thereby should emit light and electrons as the conductivity of the material increases by 2 orders of magnitude per range of $\sim$ 300 K. When heated, insulating material may exhibit conducting properties caused by thermal filling of the conduction band, thereby the mechanism of electron emission should be thermoionic like.

As submicron particles (constituing the conglomerated particle) charge themselves positively while field emitting, electric repulsion between them leads to a dislocation of the macro-particle, thus minimizing their potential energy. It has been shown that alumina bulk exploded when charged with a density of $10^{-3} - 10^{-2}$ elementary charge per molecule.[24]

8 OBSERVATION OF LIGHT SPOTS

The two types of samples (see Figure 3) have also been intentionally contaminated for light observation and measurements in the $\ll$ optical $\gg$ RF cavity (see Refs. 25, and 7 for more details).

8.1 Alumina Particles on a Cu Sample (Type #1)

When submitted to RF field (duty cycle 4 ms/800 ms), few stable light spots, whose intensity was estimated to be 10^{-13} W, appeared at 5 MV/m. The density of spots and their intensity increased with the applied field, even saturating the intensified camera. At 10 MV/m, the antenna collects a very unstable electron current (500 μA), whereas luminous tracks originating from few spots were following straight or curved trajectories (see below).

Simultaneously, one could note an increase of the pressure in the cavity accompanied with a frequency detuning. Electron and light emissions stabilize after several RF pulses. However these spectacular instabilities took place at once after a further increase of the field level, until 40 MV/m where a stable emission phase was reached. Then light spectra measurements were

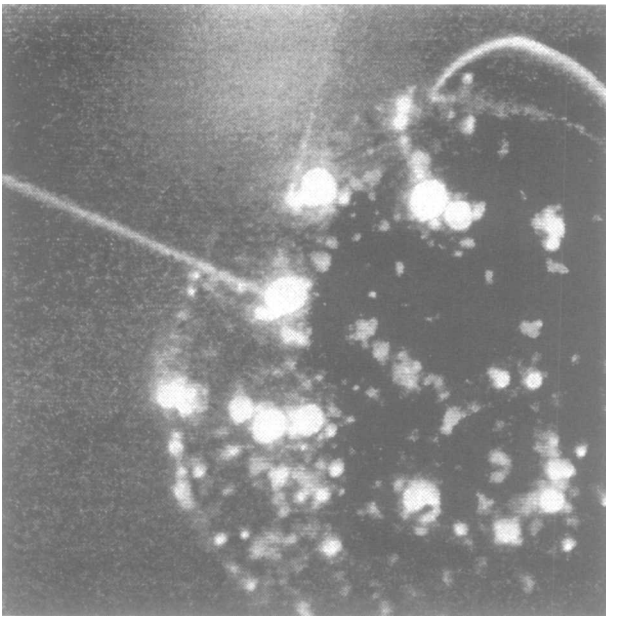

FIGURE 21 Luminous tracks originating from few spots following straight or curved trajectories.

performed on stable spots in the range 30–40 MV/m, and presented in the next figure. The maximum of spectral power ranges from 600 nm to 800 nm. Other spots revealed some multi-peaked spectra. The intensity of the spots seemed to obey the empirical law of Alfrey and Taylor for electroluminescence.[26]

8.2 Iron Particles on a Nb Sample (Type #2)

A niobium sample contaminated with iron particles has been mounted in the $\ll$ optical $\gg$ cavity, after observation in the SEM. RF test was performed with a duty cycle of 4 ms/800 ms. Many events occured during the field increasing phase:

(i) An electron field emission of 600 pA is dectected at 10 MV/m. Sudden instabilities of the current level ($\pm$ one or two orders of magnitude) indicated a processing of the sample as long as the field was increased. The highest current of 650 μA was measured at 37 MV/m, and stabilized at 46 μA at 58 MV/m.

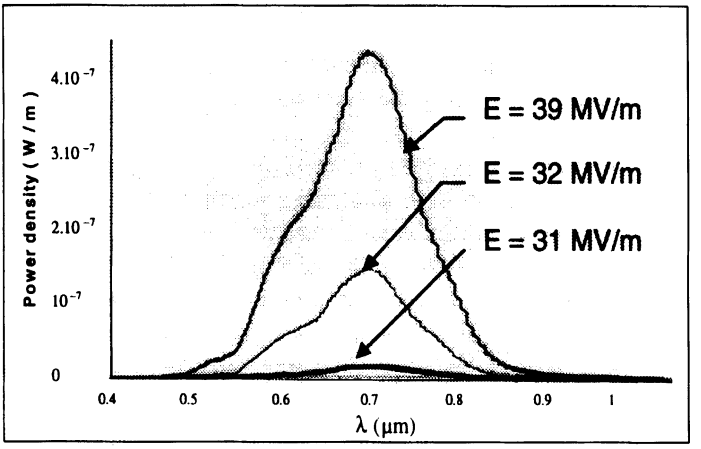

FIGURE 22 Spectra of one light spot as a function of the wavelength, at different field levels.

(ii) Particles started to move at 7.5 MV/m, being either lined up along electric field lines or ejected out of the sample surface. Note that the phenomenon is initiated at field increasing phases, and not at constant field. The motion of particles is accompanied with flashes which lasted just one RF pulse. They occured either at the sample-particle interface or at the particle-particle interface while piling up (see Figure 23). We lay emphasis on the absence of stable light spots whereas a stable FE current of 46 μA was collected at 58 MV/m.

8.3 Discussion

The main features measured from the first experiment may be interpreted through two different physical processes, i.e. electroluminescence or thermal radiation.

Electroluminescence described by some authors[26,27] occurs via a mechanism of conducting channel generation in dielectric material under electric field. Photons are emitted after electron scattering on local region of high resistivity in the channel. If one excepts the gaussian shape or bell shape of the spectra presented here, Hurley and Dooley had reported similar optical characteristics of light spots from large area electrodes submitted to high DC field. The spectra obtained by the authors were sharply peaked.

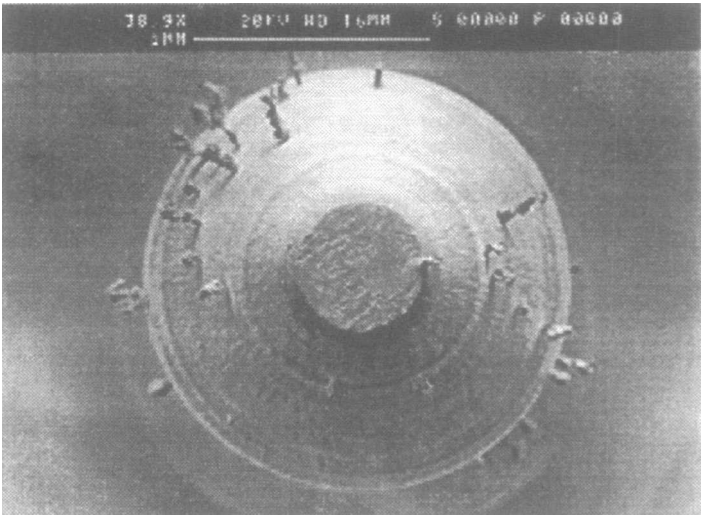

FIGURE 23 After RF test: piling of iron particles perpendicularly to the niobium sample surface.

The second mechanism involved has already been suggested in Section 7.3. Though calculations of the thermal radiation due to RF dissipation in dielectric material exhibit broad spectra in the same wavelength range, this time the wavelength at maximum intensity is related to the electric field.[25] The spectra of Figure 22 where the wavelengths at maximum power density do not seem to be field dependent, are not consistent with the second analysis.

In the case of metal contaminants, it appears clearly that electron emission is not related to light emission. Here, light spots seem to be related to transient phenomena rather than to steady state ones. In a previous experiment with a type #1 Cu sample which had been scratched, the stable light spots studied were not at all located at the geometrical defect place.[14] Moreover, a correlation was found between the spot intensity and the RF pulse length. These light spots may be due to the presence of natural insulating particulate contaminants on the sample surface. A contrario, it was established that FE current at a given field level was independent of the pulse length or duty cycle.[28] The main conclusion obtained with this experiment is that, within the sensivity of our optical facility, stabilized $\ll$ cold $\gg$ electron emission from metal sites is not accompanied with light emission by these sites.

In the next future, a series of experiments will be devoted to lighten the mechanism(s) responsible of dielectric dust behaviour under RF field described above.

9 CONCLUSIONS

This review has shown that the association of DC and RF apparati for field emission studies was very fruitful.

Confirmation of the correlation between RF field emission and surface defects is given here: dust contaminant and scratches. Special attention was drawn to dust particles as their presence on extended surfaces is hardly avoidable. Further, RF experiments have pointed out some violent processing undergone by particles intentionally sprayed on metal surfaces.

Dealing with iron particles, the new beam firing technique used for measuring the contact thermal resistance direct our interpretation of the thermal effects observed towards ion bombardment (microplasma), whereas RF dissipation seems plausible for alumina particles.

The behaviour of the latter under RF field differs fundamentally from previous DC observations where it had been shown that insulating particles do not emit electrons in DC. Our new finding is that alumina particles are strong field emitters and light emitters in RF regime. On the other hand they melt or explode into thousand of minute pieces. If high RF field may be responsible for these effects, the physical mechanism of light emission however remains unclear.

It was shown that RF pulse processing can remove dust contaminant from surfaces. A more efficient cleaning is reached by: processing with a large number of pulses to obtain a cumulative effect, favoring (if possible) short pulses to avoid thermal effects, applying a high enough peak field to overcome adherence forces.

The direct comparison of field emission in RF and DC regimes was not conclusive due to the disturbances caused by adsorbed gases. Now, as problems on DC current instabilities are solved, measurements to be undertaken in the next future should answer the following question: does the same tunneling mechanism rule RF and DC field emission?

Acknowledgements

I am very grateful to my colleagues, namely: H. Safa, B. Bonin, M. Jimenez, A. Curtoni and M. Luong at Saclay — T. Junquera, A. Le Goff, S. Maïssa and M. Fouaidy at Orsay, for many useful discussions and for kindly supplying many of the figures used in this paper.

References

[1] Noer, R.J. (1982). *Appl. Phys. A*, **28**, 1. High Voltage Vacuum Insulation: Basic Concept and Technological Practise, Ed: Latham, R.V., Academic Press, N.Y., 1995.
[2] Bernard, Ph. *et al.* (1981). *Nucl. Instrum. Methods*, **190**, 257.
[3] Curtoni, A. (1994). Ph.D Thesis, University of Orsay, France.
[4] Chianelli, C., Curtoni, A., Zeitoun-Fakiris, A., Jodet, J. and Regardin, I. (1991). *Proc. of the 5th Workshop on RF Superconductivity*, 700, Hamburg, Germany.
[5] Tan, J., Safa, H., Bonin, B. and Tessier, J.M. (1994). *J. Phys. D: Appl. Phys.*, **27**, 2644.
[6] Klein, U. and Turneaure, J.P. (1983). *IEEE Trans. Magn. MAG*, **19**, 1330.
[7] Maïssa, S., Junquera, T., Fouaidy, M., Le Goff, A., Luong, M., Tan, J., Bonin, B. and Safa, H. This Workshop.
[8] Bonin, B. (1993). *Proc. of the 6th Workshop on RF Superconductivity*, 1033, CEBAF, Newport News, USA.
[9] Mahner, E., Minatti, N., Piel, H. and Puperter, N. (1993). *Applied Surface Science*, **67**, 23.
[10] Moffat, D.L. *et al.* (1992). *Particle Accelerators*, **40**, 85.
[11] Jimenez, M., Noer, R.J., Jouve, G., Jodet, J. and Bonin, B. (1994). *J. Phys. D: Appl. Phys.*, **27**, 1038.
[12] Jimenez, M., Noer, R.J., Jouve, G., Antoine, C., Bonin, B. and Jodet, J. (1993). *J. Phys. D: Appl. Phys.*, **26**, 1503.
[13] Tan, J., Safa, H., Bonin, B. and Jimenez, M. (1994). *J. Phys. D: Appl. Phys.*, **27**, 2654.
[14] Junquera, T., Le Goff, A., Maissa, S., Bonin, B., Safa, H. and Tan, J. (1994). *Proc. of the Fourth European Particle Accelerator Conference*, London, U.K., 2203.
[15] Keldysh, L.V. (1965). *Sov. Phys. JETP*, **20**, 1307.
[16] Luong, M., Bonin, B., Long, H. and Safa, H. This Workshop.
[17] Graber, J.H. (1993). Ph.D., Thesis, Cornell University, Ithaca, N.Y.
[18] *Proc. of the 6th Workshop on RF Superconductivity*, CEBAF, Newport News, USA (1993).
[19] Bowling, R.A. (1988). *Particles on Surfaces*, p. 129, ed. K.L. Mittal, Plenum Press, NY.
[20] Tan, J., Safa, H. and Bonin, B. This Workshop.
[21] Reimer, L. *Scanning Electron Microscopy*, vol. 45, Springer-Verlag, Berlin.
[22] Pages, L., Bertel, E., Joffre, H. and Sklavenitis, L. (1970). *Pertes d'énergie, parcours et rendement de freinage pour les électrons de 10 keV à 100 MeV dans les éléments simples et quelques composés chimiques*, CEA internal report R-3942.
[23] Paulini, J., Klein, T. and Simon, G. (1993). *J. Phys. D: Appl. Phys.*, **26**, 1310.
[24] Dieumegard, D. (1995). Thomson Tubes Electroniques, Vélizy, France, private communication.
[25] Maïssa, S., Junquera, T., Fouaidy, M., Le Goff, A., Bonin, B., Luong, M., Safa, H. and Tan, J. (1995). *Proc. of IFES 95*, Madison, Wisconsin.
[26] Alfrey, G.F. and Taylor, J.B. (1955). *Brit. J. Appl. Phys.*, **4**, S44.
[27] Hurley, R.E. and Dooley, P.J. (1977). *J. Phys. D: Appl. Phys.*, **10**, L195.
[28] Tan, J. (1995). Ph.D, Thesis, *Pierre & Marie Curie University*, Paris, France.